

Relaxation of axially confined 400 GeV/c protons to planar channeling in a bent crystal: Supplementary Material

L. Bandiera¹, A. Mazzolari¹, E. Bagli¹, G. Germogli¹, V. Guidi¹,
A. Sytov^{1,6}, I. V. Kirillin², N. F. Shul'ga², A. Berra³, D. Lietti³, M.
Prest³, D. De Salvador⁴, and E. Vallazza⁵

¹INFN Sezione di Ferrara, Dipartimento di Fisica e Scienze della
Terra, Università di Ferrara Via Saragat 1, 44122 Ferrara, Italy

²Akhiezer Institute for Theoretical Physics, National Science
Center “Kharkov Institute of Physics and Technology”,
Akademicheskaya Str., 1, 61108 Kharkov, Ukraine & V.N. Karazin
Kharkov National University, Svobody Sq. 4, 61022, Kharkov,
Ukraine

³Università dell’Insubria, via Valleggio 11, 22100 Como, Italy &
INFN Sezione di Milano Bicocca, Piazza della Scienza 3, 20126
Milano, Italy

⁴INFN Laboratori Nazionali di Legnaro, Viale dell’Università 2,
35020 Legnaro, Italy & Dipartimento di Fisica, Università di
Padova, Via Marzolo 8, 35131 Padova, Italy

⁵INFN Sezione di Trieste, Via Valerio 2, 34127 Trieste, Italy

⁶Research Institute for Nuclear Problems, Belarusian State
University, Bobruiskaya street, 11, Minsk 220030, Belarus

November 11, 2015

For a better description of the process of scattering of the 400 GeV/c proton beam in the field of $\langle 111 \rangle$ axes, we present two animations of the evolution of the deflected beam distributions vs. the penetration depth inside the two tested crystals. A sketch of the strip crystals used in the experiment is shown in Fig. 1. The strip is bent via a mechanical holder that imparts a primary curvature, resulting in a secondary anticlastic curvature. This secondary curvature is used to steer the beam that impinges onto the middle of the crystal (see the big

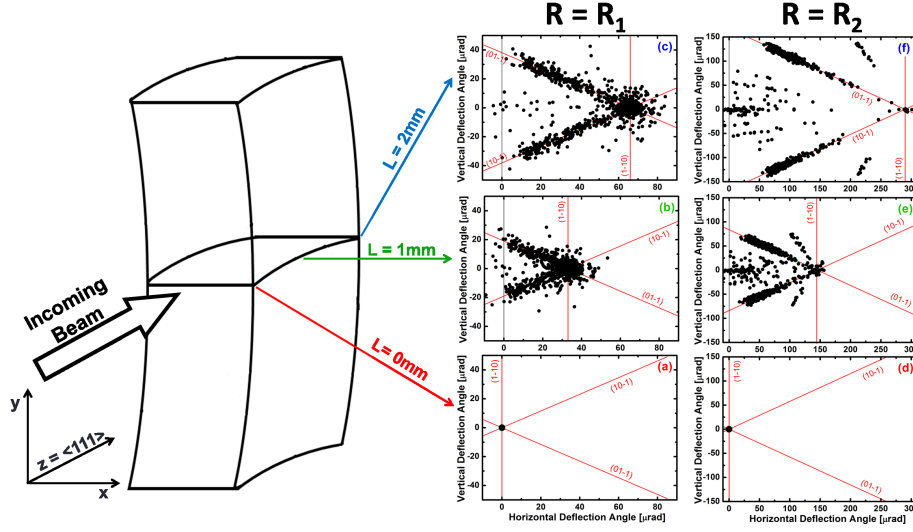


Figure 1: Left: Sketch of the strip crystals used in the experiment. The anti-clastic curvature is used to steer the beam that impinges on the crystal entry face ($1 \times 55 \text{ mm}^2$) in its center (see the big-arrow direction). Dimension not to scale. Right: Deflected beam distributions for the crystal 1 at the crystal entry face [$L = 0 \text{ mm}$, (a)], in the middle [$L = 1 \text{ mm}$, (b)] and at the crystal exit [$L = 2 \text{ mm}$, (c)]. The same for the crystal 2 are shown in plots (d) [$L = 0 \text{ mm}$], (e) [$L = 1 \text{ mm}$] and (f) [$L = 2 \text{ mm}$], respectively.

arrow in Fig. 1). The two animations have been obtained with the Monte Carlo code used in the paper and show the protons deflection angle in the plane (x, y), which is orthogonal to the $\langle 111 \rangle$ crystal axis. Each animation shows the deflected beam distribution vs. penetration depth for each frame. The red lines represent the three (110) atomic planes. Animations 1 and 2 are for the crystals with bending radii $R_1 = 30.3 \text{ m}$ and $R_2 = 6.9 \text{ m}$, respectively.

Three frames of the animations at different beam penetration depths (L), i.e., $L = 0, 1, 2 \text{ mm}$, are displayed in Fig. 1 for both R_1 (plots a, b, c) and R_2 (plots d, e, f).

A direct comparison of the two animations highlights that, at the first steps inside the crystal, most of the particles are stochastically deflected in the horizontal plane for both the crystals, while the relaxation to planar channeling in the planes intercepting the axes is more effective for crystal 2. Indeed, in this second case, after the first half of the crystal, practically all the particles left the axial region, being then captured by the planar potential wells.